Published in final edited form as:

Xray Spectrom. 2021 ; 50(1): . doi:10.1002/xrs.3183.

Valence-to-core X-ray emission spectroscopy of titanium compounds using energy dispersive detectors

Luis Miaja-Avila[1], **Galen C. O'Neil**[1], **Young Il Joe**[1], **Kelsey M. Morgan**[1], **Joseph W. Fowler**[1], **William B. Doriese**[1], **Brianna Ganly**[2], **Deyu Lu**[3], **Bruce Ravel**[4], **Daniel S. Swetz**[1], **Joel N. Ullom**[1]

[1]National Institute of Standards and Technology, Boulder, Colorado

[2]CSIRO, Sydney, Australia

[3]Center for Functional Nanomaterials, Brookhaven National Laboratory, Upton, New York

[4]National Institute of Standards and Technology, Gaithersburg, Maryland

Abstract

X-ray emission spectroscopy (XES) of transition metal compounds is a powerful tool for investigating the spin and oxidation state of the metal centers. Valence-to-core (vtc) XES is of special interest, as it contains information on the ligand nature, hybridization, and protonation. To date, most vtc-XES studies have been performed with high-brightness sources, such as synchrotrons, due to the weak fluorescence lines from vtc transitions. Here, we present a systematic study of the vtc-XES for different titanium compounds in a laboratory setting using an X-ray tube source and energy dispersive microcalorimeter sensors. With a full-width at half-maximum energy resolution of approximately 4 eV at the Ti Kβ lines, we measure the XES features of different titanium compounds and compare our results for the vtc line shapes and energies to previously published and newly acquired synchrotron data as well as to new theoretical calculations. Finally, we report simulations of the feasibility of performing time-resolved vtc-XES studies with a laser-based plasma source in a laboratory setting. Our results show that microcalorimeter sensors can already perform high-quality measurements of vtc-XES features in a laboratory setting under static conditions and that dynamic measurements will be possible in the future after reasonable technological developments.

1. INTRODUCTION

Non-resonant X-ray emission spectroscopy (XES) is a powerful technique for the study of occupied electron orbitals in the valence shell with elemental selectivity and under in situ conditions.[1–8] In XES, X-ray photons with energy greater than the binding energy of an

Correspondence Luis Miaja-Avila, National Institute of Standards and Technology, Boulder, CO 80305. miaja@nist.gov.

SUPPORTING INFORMATION

Additional supporting information may be found online in the Supporting Information section at the end of this article.

inner-shell electron produce core-hole vacancies. These core holes are quickly filled by the relaxation of less tightly bound electrons with concomitant X-ray fluorescence or emission. In first row transition metal K-edge XES, the Kα emission lines arise from 2p electrons filling 1s orbital vacancies, while the Kβ main lines, which include $K\beta_{1,3}$ and Kβ', result from 3p → 1s transitions. Additionally, the Kβ satellite or valence-to-core (vtc) spectral features, Kβ" and $K\beta_{2,5}$, result from transitions between the valence orbitals and the 1s core hole.

Traditionally, XES measurements have focused on the study of changes in the Kα and Kβ main lines for different chemical environments of the absorbing atom, where Kβ XES has proven to be sensitive to metal spin state and metal oxidation state.[6] While most of these studies have been performed on steady-state samples, the development of bright and short pulse duration X-ray sources has allowed the observation of light-induced spin state transitions in metal center coordination compounds.[9–15] Furthermore, significant progress in the study of vtc-XES has been enabled by advances in high brightness radiation sources, improvements in the collection efficiency of spectrometers, and progress in the understanding of these lines through quantum mechanical calculations.[16–18]

Vtc-XES directly reflects the electron orbital configuration that participates in the chemical bond and can be used to probe the valence electronic levels and for ligand identification, hybridization, and protonation state.[16–19] While similar information can be learned from valence band photoemission, vtc-XES has less stringent requirements on the sample environment and crystallinity. Vtc-emission lines are typically divided in two regions: Kβ" and $K\beta_{2,5}$. The Kβ" lines emerge from transitions involving valence molecular orbitals with ligand *s* atomic character and some metal p contribution, while the $K\beta_{2,5}$ lines result from transitions involving valence molecular orbitals with ligand *p* character and some metal *p* character. Furthermore, the energy separation between the Kβ" and $K\beta_{2,5}$ emission lines is associated with the difference in binding energy between the ligand *s* and *p* atomic orbitals. Vtc-XES lines have very weak fluorescence due to the small amount of metal *p*-character in the valence orbitals involved in these transitions, resulting in emission lines that can be up to three orders of magnitude weaker than the bright Kα lines.

Comparative studies of vtc-XES have been performed for different molecular complexes of first-row transition metals such as titanium,[20–23] vanadium,[24] chromium,[25,26] manganese,[27–30] iron,[16,17] and cobalt.[31] Additionally, vtc-XES has been applied to the study of 4d metals such as molybdenum[32] and niobium,[33] while groups at the Advanced Photon Source (APS) and the Linac Coherent Light Source (LCLS) extended vtc-XES to the time domain by probing the dynamics of valence electrons in iron containing complexes.[34–36]

To date, most vtc-XES measurements have been performed at high-brightness user facilities, such as synchrotrons, while a few groups have developed laboratory-based systems.[37–44] A constant in all previous vtc-XES measurements is the use of wavelength dispersive detection techniques, where specially designed gratings or crystals are used to spatially separate the different photon energies in the emission spectrum. In earlier work, we have described a tabletop apparatus capable of performing static and dynamic XES measurements in the Kα and Kβ regions using a combination of a laser-based plasma source and energy-resolving

cryogenic sensors.[45–47] In this manuscript, we report the use of these detectors for a systematic study of the vtc X-ray emission spectra for different titanium compounds. In our measurements, we resolve shifts in the Kα and $K\beta_{2,5}$ emission lines for the different titanium complexes and compare them to theoretical calculations and previously published data. Additionally, we perform calculations to assess the possibility of performing time-resolved vtc-XES measurements with our time-resolved tabletop apparatus.

2 | EXPERIMENTAL AND THEORETICAL METHODS

The samples chosen for this study are all titanium-based compounds with simple ligand geometries and different oxidation states. The samples with their respective oxidation states (in parenthesis) are: Ti metal, Ti(II)O, Ti(III) N, Ti(IV)C, and Ti(IV)O_2 in both anatase and rutile form.

Figure 1 shows a schematic of our experimental setup. The samples are commercially purchased high-purity powders packed into a 5-mm-long pressed polyimide straw with a thickness of 0.4–0.5 mm, which is then glued onto the sample holder. For calibration, we used a 2.5 × 3 × 0.5 mm^3 piece of titanium metal and a 2 × 3 × 0.5 mm^3 piece of chromium. We use a commercial X-ray tube source, with a voltage of 13.5 kV, to illuminate a six-sided sample holder where sides A through E contain a different titanium compound and side F holds the calibration targets. Each sample is individually irradiated by the source for 1 min until the sample holder is rotated to the adjacent side. The X-rays emitted from the sample are then collected by our microcalorimeter array detector, located at a distance of 7 cm from the sample.

With this sample switching technique, we can obtain XES measurements from each sample in every rotation without disturbing the environment of the microcalorimeters. This switching technique allows us to perform a simultaneous calibration, which is often used with microcalorimeter detectors, where in every rotation we measure calibration lines while also measuring multiple different samples whose XES lines sometimes overlap with the calibration lines. We assign a systematic uncertainty of 50 meV to line energies measured with this technique (see the Supplementary Information [Data S1] for more details and a discussion of the source and magnitude of this systematic uncertainty and the calibration process). The XES spectra presented in this study were obtained over a period of 3 days where the total acquisition time for each individual titanium compound is approximately 10 hr.

The cryogenic transition-edge sensor (TES) microcalorimeter array spectrometer used to measure the X-ray spectrum from each compound is similar to spectrometers that have been previously described in detail.[48–51] Briefly, the spectrometer consists of 192 superconducting TESs, each biased in the middle of its superconducting transition at approximately 0.115 K. An X-ray incident upon a sensor causes a temperature rise, which causes a drop in current through the sensor. The sensor relaxes back to its quiescent temperature in a few milliseconds. The current transient induced by the absorbed X-ray is measured and analyzed to determine the magnitude of the X-ray energy with a resolving power greater than 1,000. The pulse magnitude in arbitrary units is converted to energy

using an interpolating spline built from the fixed points determined from the Kα and Kβ lines of metallic Ti and Cr.[52–54] The array is read out with time-division multiplexing.[49] Each pixel consists of a Mo-Cu bilayer with an Au sidecar absorber on a SiN membrane. This Au sidecar absorber is the primary difference from previously described spectrometers; it allows a nearly perfectly Gaussian detector response function, where previously described spectrometers had significant low energy tails.[55] In these results, we observed one noteworthy deviation from a Gaussian detector response, which is the appearance of a spurious spectral feature roughly 70 eV below each true feature. The spectral artifact is broader than its parent feature and has about 1.5% of its intensity. The artifact is caused by photons that pass through the metal of a TES sensor and are absorbed in the SiN underneath, resulting in incomplete and variable energy capture. The chief effect of this artifact is to obscure radiative Auger features[56,57] whose energy location is regrettably similar.

The vtc-XES spectra of all the Ti compounds (Ti metal, TiO_2 anatase and rutile, TiO, TiN, and TiC) were simulated using the OCEAN package.[58,59] Kohn-Sham orbital energies and wavefunctions needed to compute the XES coefficients were calculated from the Quantum ESPRESSO package[60] using the local density approximation in the norm-conserving pseudo-potential implementation. A kinetic energy cutoff of 100 Rydberg was used for the wavefunction. Calculations of Ti compounds were performed on their experimental structures[61] obtained from the Crystallography Open Database.[62,63] The same unit cells as those in the database were used in the spectral simulations except for TiN and TiC, where the primitive cells of the face-centered cubic lattice (1/4 of the conventional cell volume) were used. In the self-consistent calculations, the Brillouin zone was sampled with k-point meshes of 16 × 16 × 10 for Ti metal, 8 × 8 × 4 for TiO_2 (anatase), 6 × 6 × 9 for TiO_2 (rutile), 8 × 6 × 8 for TiO, 10 × 10 × 10 for TiN, and 16 × 16 × 16 for TiC to obtain the ground state density. In the subsequent non self-consistent calculations, denser k-point meshes were used (26 × 26 × 16, 12 × 12 × 6, 10 × 10 × 15, 16 × 12 × 16, 20 × 20 × 20, and 26 × 26 × 26) to sample the valence band structure used to compute transition matrix elements. The projected density of states (PDOS) were used to make peak assignment, which were broadened with a Lorentzian function with a full-width at half-maximum (FWHM) of 0.2 eV (as shown in Figure S3). To make a direct comparison between theory and the microcalorimeter data, the calculated XES spectra were broadened with a Gaussian function with FWHM of 4 eV to account for instrument broadening, and an empirical energy-dependent Lorentzian function with FWHM = 0.94 + ($E_f - E$)/12 eV, where E_f is the Fermi level and E is the energy of the valence band states. The constant and the linear terms in the Lorentzian width account for the Ti 1s core-hole lifetime[64] and excited state lifetime, respectively. This broadening scheme has been used in common X-ray spectroscopy codes[65,66] and in the study of Nb vtc-XES.[33]

3 | RESULTS AND DISCUSSION

Figure 2 shows the microcalorimeter XES spectra of all the different samples in this study, where the most prominent features in the spectra are the Kα and Kβ main and satellite peaks. The displayed 700 eV energy region has an energy resolution of 3.8 ± 0.1 eV in the Kα region and 4.0 ± 0.1 eV in the Kβ region. From left to right, the features visible in the spectra are: (A) a detector artifact about 70 eV below the $Kα_2$ lines due to Kα photons that

pass through the metal of the TES sensor and are absorbed in the SiN underneath, (B) the $K\alpha_{1,2}$ lines at 4510.9 eV ($K\alpha_1$) and 4,505.9 eV ($K\alpha_2$) for the pure Ti metal sample,[52] (C) the Kα satellite ($K_\alpha L^1$), at about 30 eV above the $K\alpha_1$ lines,[56,57,67] (D) the same detector artifact from the Kβ complex, (E) the Kβ' line, (F) the $K\beta_{1,3}$ lines at 4931.8 ($K\beta_1$) for the pure Ti metal sample,[53] (G) the Kβ" lines, (H) the $K\beta_{2,5}$ lines, and (I) the $K_\beta L^1$ peaks, a few eV above the $K\beta_{2,5}$ lines. As shown in these measurements, the energy-resolving capabilities of the microcalorimeter array detectors allow us to measure the entire XES spectrum simultaneously and resolve features, which are orders of magnitude weaker than the bright Kα lines, without sacrificing collection efficiency or having to recalibrate the detector for different energy regions.

As previously mentioned, the focus of this manuscript is to measure changes in the vtc-XES spectra for the different titanium compounds. In a brief digression, we take the opportunity to compare the Kα regions to previously published results. The Kα region of the spectrum is known to contain information concerning the effective charge of the metal center. As can be seen in Figure 3a, we clearly observe a chemical shift of the $K\alpha_1$ and $K\alpha_2$ peaks for the different titanium compounds, where the shift is dependent on both the oxidation number and the number of unpaired electrons. Figure 3b shows the measured shift of the $K\alpha_1$ peaks of the different compounds with respect to the titanium metal $K\alpha_1$ peak. The location of the $K\alpha_1$ peak was obtained by fitting Voigt functions to the XES data after background subtraction. To compare our results, we also display previously published high-resolution titanium $K\alpha_1$ XES shifts.[68] Our measurements are consistent with the idea that the $K\alpha_1$ shift to lower energy correlates with the decrease of 3d electron density on the titanium atom. It is important to point out that although the energy resolution in this region of the spectrum is 3.8 ± 0.1 eV we can still distinguish the small peak shifts ranging from 0.1 to 0.8 eV because the uncertainty of our $K\alpha_1$ locations is ±0.05 eV. The source of these uncertainty values is primarily systematic, see Supplementary Information (Data S1) for a detailed discussion.

We return to the Kβ region, which is known to contain more information on the chemical state of the sample.[4,6,16–18] This part of the spectrum is typically divided into two regions: the Kβ main lines (Kβ' and $K\beta_{1,3}$), dominated by spin state contributions, and the Kβ satellite or vtc region (Kβ" and $K\beta_{2,5}$), which is very sensitive to the effects of the ligands. Figure 4a shows the entire Kβ region for all the measured compounds, while Figure 4b focuses on the vtc-XES region. The data presented in these two figures has been normalized to the total counts in the Kβ region of the spectrum, which we defined as 4,900 to 4,980 eV. The energy resolution in this region of the spectrum is 4.0 ± 0.1 eV, which is about an order of magnitude worse than what can be obtained with wavelength dispersive techniques (~0.5 eV). However, the microcalorimeter data presented in Figure 4b clearly resolves the $K\beta_{2,5}$ emission lines for all the titanium compounds and even the dim Kβ" peak can be observed in the TiO_2 spectra (both anatase and rutile) and in the TiC spectrum where the energy separation between the Kβ" and $K\beta_{2,5}$ is as small as 7 eV. Additionally, Figure 4c shows the OCEAN vtc-XES spectra for the different Ti compounds after including a core-hole lifetime broadening of 0.94 eV,[64] a linear Lorentzian broadening to include the lifetime of the excited states, and an instrument broadening of 4.0 eV to account for the energy resolution of the microcalorimeter array detectors in this region of the spectrum. Overall,

panels 4b and 4c show very good agreement between the microcalorimeter array detector data and the OCEAN simulations.

To explore what information might be lost by using detectors with 4 eV energy resolution, we modified our broadening scheme of the OCEAN spectra during the post-processing to consider only core-hole and quasi-particle lifetime broadening as an energy-dependent Lorentzian broadening; therefore, simulating the kind of spectra that could be obtained with a very high-resolution spectrometer. The results of these calculations are presented in Figure 4d, where the data illustrates that for most Ti compounds the TES spectra shows the same features as the lifetime-broadened OCEAN spectra, with the obvious difference that the peaks in the TES data are wider due to the detector's 4 eV energy resolution. However, the spectra for TiO_2 (both anatase and rutile) show fine $K\beta_{2,5}$ features that can only be observed in the OCEAN simulated data originated from the Ti 3d and O 2p hybridization as shown in the PDOS (see Figure S3), but not in the TES spectra. These comparisons show that while TES detectors are able to perform vtc-XES spectroscopy in simple transition metal compounds, further improvements in their energy resolution are needed to observe all the intricate details in vtc-XES.

Furthermore, and to better understand the effects of an energy resolution of 4 eV in the data analysis and peak assignment, we performed vtc-XES measurements of the same Ti compounds at a synchrotron beamline, where the detection technique was based on wavelength dispersive elements and a CCD camera. In Figure S2, we present a comparison of our microcalorimeter array data to the synchrotron data for all titanium compounds. As expected, the peaks in the microcalorimeter data are broader than the ones from the synchrotron data, but the presence of the different vtc features are still clearly observable in the microcalorimeter data.

A noticeable feature in Figure 4 is an energy shift of the Kβ" and $K\beta_{2,5}$ lines for the different titanium compounds. To quantify this shift, we used a least-squares fitting program to fit all the features in the Kβ region of the spectra. In our model, the Kβ', $K\beta_{1,3}$, Kβ", and $K\beta_{2,5}$ peaks were represented as Voigt functions, while the detector artifact from SiN events and the $K_\beta L^1$ peak were described by Gaussian functions, and the background was represented by a linear function. Similarly to Mandić et al.[21] we introduced another Voigt function peak between the Kβ' and $K\beta_{1,3}$ peaks. Based on this analysis, Table 1 shows the energy separation between the $K\beta_{1,3}$ and $K\beta_{2,5}$ peaks as a function of the oxidation state of the different titanium compounds obtained with our microcalorimeter array, the synchrotron measurements, OCEAN simulations, and previously published results.[21,23] Our results using microcalorimeter array detectors are consistent with the previously published values except for one compound, TiN.[21] These results are significant since the energy resolution of the spectrometer used for the synchrotron measurements is better than 1 eV[69] (0.5–0.9 eV) while the energy resolution of our detectors is ~4 eV; nonetheless, we are able to observe the same vtc features and measure the correct peak energy position and energy separations. Moreover, the energy separation uncertainties between the synchrotron and microcalorimeter data are very similar, although a disadvantage of the microcalorimeter data is that its acquisition time was ~100× longer. The Supplementary Information (Data S1) section contains a discussion on the uncertainty values presented in Table 1.

In the case of TiN, the energy difference between the $K\beta_{1,3}$ and $K\beta_{2,5}$ peaks using microcalorimeter array detectors is 27.4 ± 0.1 eV, 27.8 ± 0.1 eV was measured at the synchrotron, and 28.2 eV was obtained through the OCEAN simulations, while 31.6 ± 0.5 eV is the published value.[21] TiN has an oxidation state of III, so the expected energy difference should fall in between the values for samples with oxidation state of II (~26 eV) and the one for samples with oxidation state of IV (~30 eV). The value of 31.6 ± 0.5 eV from Mandić et al.[21] seems to be closer to values expected from samples with a higher oxidation state, while the energy differences measured with the microcalorimeter detectors (27.4 ± 0.1 eV) and the one from the synchrotron (27.8 ± 0.1 eV) seem to follow the linear trend from Table 1. Therefore, we believe that our energy difference values for TiN, which were complemented by synchrotron measurements and OCEAN simulations, are closer to the true values.

In the following paragraphs, we consider the application of a TES spectrometer to more experimentally challenging variations on vtc measurements, such as time-resolved vtc-XES studies. The capability to observe femtosecond to picosecond dynamics in the vtc region of the XES spectrum, which elucidates ultrafast valence band dynamics in metal-centered molecular complexes, has recently been reported by groups at the APS[35] and the LCLS.[36] However, access to large-scale facilities that can perform these time-resolved experiments is limited to just a few worldwide. Expanding time-resolved capabilities to smaller-scale facilities would require the use of tabletop X-ray sources[45,70,71] and extremely efficient X-ray detectors. We have previously shown that using a laser-based plasma source and these microcalorimeter array detectors we can observe changes in the Kα and Kβ main regions of the spectrum on ps-timescales.[47] In such measurements, obtaining a set of ground-state (low-spin [LS]) and laser-excited spectra per time delay took roughly 12 hr. Since the vtc-XES features are about an order of magnitude dimmer than the $K\beta_{1,3}$ features, we use the steady-state results presented in this manuscript to perform calculations and explore the possibility of achieving a study of vtc-XES dynamics in a laboratory setting. These calculations assume the use of an apparatus based on a 20 mJ Ti:Sapphire laser system, a laser-based plasma source with a 100-μm water jet as the target, a polycapillary X-ray optic, and a microcalorimeter array detector. In our calculations, we assume the sample to be in the LS state (ground state) and after irradiation with an ultrafast light pulse the sample transitions to a laser-excited state, which is a combination of high-spin (HS) and LS states. While spin crossover (SCO) can often be observed using other spectral features, we take SCO as a representative example of a range of dynamic vtc-XES studies because of the recent availability of experimental demonstrations. Based on the data presented by March et al.,[35] we assume the amplitude of the HS state vtc features to be ~60% of the LS state vtc features and that the position of the HS vtc features is 1.8 eV higher than the LS features. Additionally, we assume the excitation fraction to be 30%. Therefore, the laser-excited (pump) spectra are obtained by: Pump = (1 − 0.3)LS + 0.3HS. For our calculations, we used the TiO_2 (anatase) XES data to create our model for the LS spectrum, where the model is based on a combination of Voigt, Gaussian, and linear functions as previously described. The $K\beta_{1,3}$ peak height and Kβ background level in our model were chosen to match the values obtained in our previous time-resolved measurements.[47] We then varied the number

of X-rays collected to simulate longer acquisition times and added Poisson noise to model experimental noise.

Figure 5a shows simulated spectra for the LS, HS, and laser-excited states with a total of ~1×10^7 counts in the vtc region of the spectra, where ~3×10^6 of those counts belong to X-ray emission features and the rest of the counts are from scattered Bremsstrahlung photons. This scattered signal comes from Bremsstrahlung X-rays from the source that transmit through the polycapillary X-ray optic, scatter off the sample, and make it into the detector. In Figure 5a, the difference between the ground (LS) state and pumped data is visible by eye and the signal-to-noise ratio of the difference between the pumped and LS spectra in the bins with the largest signal exceeds 5-sigma. We fit the simulated data with the pump model used to generate the data, holding all parameters fixed except for the excitation fraction. When doing this fit, we find the HS fraction to be 30.6 ± 1.6%, consistent with the correct value of 30%. In the following discussion, we assume that determining the excitation fraction to ± ~1.6% is the necessary threshold for a high quality dynamic vtc measurement. With these simulations, we can better understand how sensitive the measurements of low intensity $K\beta_{2,5}$ and Kβ" features are to the more intense scattered Bremsstrahlung photons. Therefore, our next step was to perform similar simulations but now with the scattered signal set to zero. Figure 5b shows our results with zero scattered photons, where the total number of counts is ~5×10^5 (all of them from vtc XES features) and after fitting for the excitation fraction, we find an HS fraction of 31.0 ± 1.8%. A conclusion from these simulations is that reducing the scattered Bremsstrahlung signal to zero, which could be achieved by monochromatizing the X-rays incident on the sample (at a value that differs from the vtc transition energies) thus removing the scattered Bremsstrahlung photons, would enable a measurement of similar quality with 5× fewer vtc XES photons and the interpretation would be less model dependent.

These simulations allow us to explore the possibility of performing tabletop time-resolved vtc-XES measurements. With our existing apparatus, it would take approximately 3,000 hr to collect the 10^7 vtc photons necessary to achieve a 1.6% uncertainty on the excitation fraction per time delay. Let us next consider the acquisition time with an improved apparatus based upon a metal jet X-ray source and a monochromatic X-ray optic. Laser-based plasma sources with 50× more X-ray flux than our water-jet plasma source have already been developed[70–72] and are becoming commercial products. Such a source could feature emission lines at ~8 keV (copper Kα), ~9 keV (gallium Kα) or ~11 keV (bismuth Lα) with significant intensity and X-ray fluorescence production cross section[73] across most of the first-row transition metals. Another crucial element of this proposed apparatus would be a monochromatic X-ray optic whose purpose is to transmit a specific bandwidth around the source's emission line, therefore, eliminating or greatly reducing the scattered Bremsstrahlung signal. Additionally, the optic should have a high X-ray reflectivity and/or collection efficiency. Multilayer mirrors based on a Montel design[74] contain some desirable characteristics as they are monochromatic hard X-ray optics with high X-ray reflectivity and acceptable collection efficiency. While such optic would have a transmission and focusing efficiency of about one eighth of that from a polycapillary optic, the advantage of transmitting no X-rays at the emission energies of interest is very important since it simplifies the fitting procedure and data analysis.

Compton scattering in the sample is a possible additional source of background photons that would not be mitigated by an optic. However, for likely geometries and excitation energies, Compton scattering as background is only possible when the XES features of interest are close in energy (within a few hundreds of eVs) to the X-ray source's line emission. A Compton background can be mitigated by shifting the microcalorimeter array to a different angle relative to the exciting beam.

Further improvements are possible beyond the source and optic. For example, count rates can be increased by a factor of ~4× by reducing the sample-to-detector distance, or by another ~5× with a significantly larger TES array. Additionally, we could increase the signal to noise ratio by using newly developed detectors with ~2× better energy resolution.[75] The combination of all these improvements to our apparatus would allow a spectrum such as that in Figure 5b to be acquired in approximately three to four hr. Even if our estimates are off by a combined factor up to ~10× the acquisition times remain reasonable for a tabletop experiment. Consequently, we believe that tabletop systems using bright monochromatic X-ray sources and highly efficient energy-resolving detectors could perform time-resolved vtc XES measurement in the near future.

Finally, the purpose of this work was to demonstrate that microcalorimeter array detectors have gone through extensive improvements to the point that they are now capable of measuring faint XES features, such as the vtc emission lines, even when using low brightness laboratory-based X-ray sources. While the energy resolution of microcalorimeter array detectors is not as good as what can be obtained with crystal spectrometers, it is enough to distinguish subtle variations in the vtc-XES features of different chemical compounds.

A detailed assessment of the merits of microcalorimeter array and crystal spectrometer detectors is beyond the scope of this paper but we can identify some key points of comparison. While the energy resolution of crystal spectrometers is usually better, we have shown that the energy resolution of microcalorimeters is already good enough for some vtc spectroscopies and the photon collection efficiency of microcalorimeter arrays is significantly higher than crystals as discussed in Uhlig et al.[76] This efficiency advantage is most relevant for faint X-ray sources or radiation-sensitive samples. With a strong enough X-ray source and a radiation-resistant sample, crystal spectrometers can still have shorter acquisition times because of saturation effects in microcalorimeters at high photon fluxes. Improving microcalorimeter resolution and throughput is an active area of research.[77] Unlike crystal spectrometers, microcalorimeters can measure large spectral ranges as shown in Figure 2 without sacrificing energy resolution or collection efficiency. Broadband measurements are beneficial when measuring multiple spectral features, for instance from complex samples containing multiple elements. However, a potential drawback of sensitivity over a large spectral range is the contribution of uninteresting out-of-band photons to detector saturation. In summation, the choice of detector for a particular measurement depends not only on detector properties but also on the source, sample, and science goals.

4 | CONCLUSION

We have presented a comprehensive comparison study of multiple titanium compounds using a commercial X-ray source and an array of microcalorimeter array detectors. With these detectors we measured the entire XES spectrum from the Kα emission up to the high energy Kβ satellite peaks with an energy resolution ranging from 3.8 to 4.0 eV. Even though our energy resolution is about an order of magnitude worse than what can be obtained with a traditional wavelength dispersive detector scheme, we demonstrated that our detectors are capable of observing shifts in the $K\alpha_1$ peaks and subtle differences in the dim vtc XES features for all the different titanium compounds. In addition to comparing our data to new synchrotron measurements and previously published results, we performed OCEAN simulations to understand the molecular orbital contributions to the vtc-XES features. Finally, we performed calculations of the experimental acquisition times required for laboratory-based time-resolved vtc-XES measurements using a laser-plasma X-ray source and an array of microcalorimeter array detectors. These calculations suggest that time-resolved measurements of vtc-XES features will be possible using a more optimized tabletop apparatus.

Supplementary Material

Refer to Web version on PubMed Central for supplementary material.

ACKNOWLEDGEMENTS

We gratefully acknowledge the financial support from the NIST Innovations in Measurement Science Program. This research used resources of the Advanced Photon Source, a U.S. Department of Energy (DOE) Office of Science User Facility operated for the DOE Office of Science by Argonne National Laboratory under Contract No. DE-AC02-06CH11357; the Center for Functional Nanomaterials, which is a U.S. DOE Office of Science Facility, at Brookhaven National Laboratory under Contract No. DE-SC0012704; and the National Energy Research Scientific Computing Center (NERSC), a U.S. Department of Energy Office of Science User Facility operated under Contract No. DE-AC02-05CH11231.

Funding information

Center for Functional Nanomaterials, which is a U.S. DOE Office of Science Facility, at Brookhaven National Laboratory, Grant/Award Number: DE-SC0012704; National Energy Research Scientific Computing Center (NERSC), a U.S. Department of Energy Office of Science User Facility, Grant/Award Number: DE-AC02-05CH11231; NIST Innovations in Measurement Science Program; U.S. Department of Energy (DOE) Office of Science User Facility operated for the DOE Office of Science by Argonne National Laboratory, Grant/Award Number: DE-AC02-06CH11357

REFERENCES

[1]. de Groot F, Chem. Rev. 2001, 101(6), 1779–1808. 10.1021/cr9900681. [PubMed: 11709999]

[2]. Glatzel P, Bergmann U, Coord. Chem. Rev 2005, 249(1–2), 65–95. 10.1016/j.ccr.2004.04.011.

[3]. Glatzel P, Sikora M, Smolentsev G, Fernández-García M, Catal. Today 2009, 145(3–4), 294–299. 10.1016/j.cattod.2008.10.049.

[4]. Bergmann U, Glatzel P, Photosynth. Res. 2009, 102(2–3), 255–266. 10.1007/s11120-009-9483-6. [PubMed: 19705296]

[5]. Rovezzi M, Glatzel P, Semicond. Sci. Technol. 2014, 29, 023002. 10.1088/0268-1242/29/2/023002.

[6]. Pollock CJ, Delgado-Jaime MU, Atanasov M, Neese F, DeBeer S, J. Am. Chem. Soc. 2014, 136(26), 9453–9463. 10.1021/ja504182n. [PubMed: 24914450]

[7]. Wolny JA, Schünemann V, Németh Z, Vankó G, Comptes Rendus Chim. 2018, 21(12), 1152–1169. 10.1016/j.crci.2018.10.001.

[8]. Schoch A, Burkhardt L, Schoch R, Stührenberg K, Bauer M, Faraday Discuss. 2019, 220, 113–132. 10.1039/c9fd00070d. [PubMed: 31532420]

[9]. Vankó G, Glatzel P, Pham V-T, Abela R, Grolimund D, Borca CN, Johnson SL, Milne CJ, Bressler C, Angew. Chem. Int. Ed. Engl. 2010, 49(34), 5910–5912. 10.1002/anie.201000844. [PubMed: 20818772]

[10]. Haldrup K, Vankó G, Gawelda W, Galler A, Doumy G, March AM, Kanter EP, Bordage A, Dohn A, Van Driel TB, et al., J. Phys. Chem. A 2012, 116, 9878–9887. 10.1021/jp306917x. [PubMed: 22970732]

[11]. Zhang W, Alonso-Mori R, Bergmann U, Bressler C, Chollet M, Galler A, Gawelda W, Hadt RG, Hartsock RW, Kroll T, Kjær KS, Kubiček K, Lemke HT, Liang HW, Meyer DA, Nielsen MM, Purser C, Robinson JS, Solomon EI, Sun Z, Sokaras D, van Driel TB, Vankó G, Weng TC, Zhu D, Gaffney KJ, Nature 2014, 509(7500), 345–348. 10.1038/nature13252. [PubMed: 24805234]

[12]. Kern J, Tran R, Alonso-Mori R, Koroidov S, Echols N, Hattne J, Ibrahim M, Gul S, Laksmono H, Sierra RG, Gildea RJ, Han G, Hellmich J, Lassalle-Kaiser B, Chatterjee R, Brewster AS, Stan CA, Glöckner C, Lampe A, DiFiore D, Milathianaki D, Fry AR, Seibert MM, Koglin JE, Gallo E, Uhlig J, Sokaras D, Weng TC, Zwart PH, Skinner DE, Bogan MJ, Messerschmidt M, Glatzel P, Williams GJ, Boutet S, Adams PD, Zouni A, Messinger J, Sauter NK, Bergmann U, Yano J, Yachandra VK, Nat. Commun. 2014, 5, 4371. 10.1038/ncomms5371. [PubMed: 25006873]

[13]. Wernet P, Kunnus K, Josefsson I, Rajkovic I, Quevedo W, Beye M, Schreck S, Grübel S, Scholz M, Nordlund D, Zhang W, Hartsock RW, Schlotter WF, Turner JJ, Kennedy B, Hennies F, de Groot FMF, Gaffney KJ, Techert S, Odelius M, Föhlisch A, Nature 2015, 520(7545), 78–81. 10.1038/nature14296. [PubMed: 25832405]

[14]. Alonso-Mori R, Sokaras D, Zhu D, Kroll T, Chollet M, Feng Y, Glownia JM, Kern J, Lemke HT, Nordlund D, Robert A, Sikorski M, Song S, Weng TC, Bergmann U, Synchrotron Radiat J. 2015, 22(3), 612–620. 10.1107/S1600577515004488.

[15]. Canton SE, Kjær KS, Vankó G, van Driel TB, Adachi S, Bordage A, Bressler C, Chabera P, Christensen M, Dohn AO, Galler A, Gawelda W, Gosztola D, Haldrup K, Harlang T, Liu Y, Møller KB, Németh Z, Nozawa S, Pápai M, Sato T, Sato T, Suarez-Alcantara K, Togashi T, Tono K, Uhlig J, Vithanage DA, Wärnmark K, Yabashi M, Zhang J, Sundström V, Nielsen MM, Nat. Commun. 2015, 6, 6359. 10.1038/ncomms7359. [PubMed: 25727920]

[16]. Lee N, Petrenko T, Bergmann U, Neese F, Debeer S, J. Am. Chem. Soc. 2010, 132(28), 9715–9727. 10.1021/ja101281e. [PubMed: 20578760]

[17]. Pollock CJ, Debeer S, J. Am. Chem. Soc. 2011, 133(14), 5594–5601. 10.1021/ja200560z. [PubMed: 21417349]

[18]. Gallo E, Glatzel P, Adv. Mater. 2014, 26(46), 7730–7746. 10.1002/adma.201304994. [PubMed: 24861500]

[19]. Pollock CJ, DeBeer S, Acc. Chem. Res. 2015, 48(11), 2967–2975. 10.1021/acs.accounts.5b00309. [PubMed: 26401686]

[20]. Reinhardt F, Beckhoff B, Eba H, Kanngiesser B, Kolbe M, Mizusawa M, Muüller M, Pollakowski B, Sakurai K, Ulm G, Anal. Chem. 2009, 81(5), 1770–1776. 10.1021/ac8018069. [PubMed: 19203285]

[21]. Mandíc L, Fazinić S, Jakšić M, Phys. Rev. A 2009, 80(4), 042519. 10.1103/PhysRevA.80.042519.

[22]. Swarbrick JC, Kvashnin Y, Schulte K, Seenivasan K, Lamberti C, Glatzel P, Inorg. Chem. 2010, 49(18), 8323–8332. 10.1021/ic100755t. [PubMed: 20831281]

[23]. Wansleben M, Vinson J, Holfelder I, Kayser Y, Beckhoff B, X-Ray Spectrom. 2018, 48(2), 102–106. 10.1002/xrs.3000.

[24]. Rees JA, Bjornsson R, Schlesier J, Sippel D, Einsle O, DeBeer S, Angew. Chem. Int. Ed. 2015, 54(45), 13249–13252. 10.1002/anie.201505930.

[25]. Macmillan SN, Walroth RC, Perry DM, Morsing TJ, Lancaster KM, Inorg. Chem. 2015, 54(1), 205–214. 10.1021/ic502152r. [PubMed: 25496512]

[26]. Zeeshan F, Hoszowska J, Dousse JC, Sokaras D, Weng TC, Alonso-Mori R, Kavčič M, Guerra M, Sampaio JM, Parente F, Indelicato P, Marques JP, Santos JP, X-Ray Spectrom. 2019, 48(5), 351–359. 10.1002/xrs.3019.

[27]. Bergmann U, Horne CR, Collins TJ, Workman JM, Cramer SP, Chem. Phys. Lett. 1999, 302(1–2), 119–124. 10.1016/S0009-2614(99)00095-0.

[28]. Smolentsev G, Soldatov AV, Messinger J, Merz K, Weyhermüller T, Bergmann U, Pushkar Y, Yano J, Yachandra VK, Glatzel P, J. Am. Chem. Soc. 2009, 131(36), 13161–13167. 10.1021/ja808526m. [PubMed: 19663435]

[29]. Pushkar Y, Long X, Glatzel P, Brudvig GW, Dismukes GC, Collins TJ, Yachandra VK, Yano J, Bergmann U, Angew. Chem. Int. Ed. 2010, 49(4), 800–803. 10.1002/anie.200905366.

[30]. Rees JA, Martin-Diaconescu V, Kovacs JA, DeBeer S, Inorg. Chem. 2015, 54(13), 6410–6422. 10.1021/acs.inorgchem.5b00699. [PubMed: 26061165]

[31]. Schwalenstocker K, Paudel J, Kohn AW, Dong C, Van Heuvelen KM, Farquhar ER, Li F, Dalt. Trans. 2016, 45(36), 14191–14202. 10.1039/c6dt02413k.

[32]. Doonan CJ, Zhang L, Young CG, George SJ, Deb A, Bergmann U, George GN, Cramer SP, Inorg. Chem. 2005, 44 (8), 2579–2581. 10.1021/ic050129f. [PubMed: 15819540]

[33]. Ravel B, Kropf AJ, Yang D, Wang M, Topsakal M, Lu D, Stennett MC, Hyatt NC, Phys. Rev. B 2018, 97(12), 125139. 10.1103/PhysRevB.97.125139.

[34]. March AM, Assefa TA, Bressler C, Doumy G, Galler A, Gawelda W, Kanter EP, Németh Z, Pápai M, Southworth SH, et al., J. Phys. Chem. C 2015, 119(26), 14571–14578. 10.1021/jp511838q.

[35]. March AM, Assefa TA, Boemer C, Bressler C, Britz A, Diez M, Doumy G, Galler A, Harder M, Khakhulin D, Németh Z, Pápai M, Schulz S, Southworth SH, Yavaş H, Young L, Gawelda W, Vankó G, J. Phys. Chem. C 2017, 121(5), 2620–2626. 10.1021/acs.jpcc.6b12940.

[36]. Ledbetter K, Reinhard ME, Kunnus K, Gallo A, Britz A, Biasin E, Glownia JM, Nelson S, van Driel TB, Weninger C, et al., J. Chem. Phys. 2020, 152, 074203. 10.1063/1.5139441.

[37]. Legall H, Stiel H, Schnürer M, Pagels M, Kanngieer B, Müller M, Beckhoff B, Grigorieva I, Antonov A, Arkadiev V, et al., J. Appl. Crystallogr. 2009, 42(4), 572–579. 10.1107/S0021889809006803.

[38]. Anklamm L, Schlesiger C, Malzer W, Grötzsch D, Neitzel M, Kanngießer B, Rev. Sci. Instrum. 2014, 85(5), 053110. 10.1063/1.4875986.

[39]. Seidler GT, Mortensen DR, Remesnik AJ, Pacold JI, Ball NA, Barry N, Styczinski M, Hoidn OR, Rev. Sci. Instrum. 2014, 85(11), 113906. 10.1063/1.4901599.

[40]. Németh Z, Szlachetko J, Bajnóczi ÉG, Vankó G, Rev. Sci. Instrum. 2016, 87(10), 103105. 10.1063/1.4964098.

[41]. Holden WM, Hoidn OR, Ditter AS, Seidler GT, Kas J, Stein JL, Cossairt BM, Kozimor SA, Guo J, Ye Y, Marcus MA, Fakra S, Rev. Sci. Instrum. 2017, 88(7), 073904. 10.1063/1.4994739.

[42]. Mortensen DR, Seidler GT, Ditter AS, Glatzel P, J. Phys. Conf. Ser. 2016, 712(1), 012036. 10.1088/1742-6596/712/1/012036.

[43]. Malzer W, Grötzsch D, Gnewkow R, Schlesiger C, Kowalewski F, Van Kuiken B, Debeer S, Kanngießer B, Rev. Sci. Instrum. 2018, 89(11), 113111. 10.1063/1.5035171.

[44]. Jahrman EP, Holden WM, Ditter AS, Mortensen DR, Seidler GT, Fister TT, Kozimor SA, Piper LFJ, Rana J, Hyatt NC, Stennett MC, Rev. Sci. Instrum. 2019, 90(2), 024106. 10.1063/1.5049383.

[45]. Miaja-Avila L, O'Neil GC, Uhlig J, Cromer CL, Dowell ML, Jimenez R, Hoover a. S., Silverman KL, Ullom JN, Struct. Dyn. 2015, 2(2), 024301. 10.1063/1.4913585.

[46]. Joe YI, O'Neil GC, Miaja-Avila L, Fowler JW, Jimenez R, Silverman KL, Swetz DS, Ullom JN, J. Phys. B At. Mol. Opt. Phys. 2016, 49(0), 024003. 10.1088/0953-4075/0/0/000000.

[47]. Miaja-Avila L, O'Neil GC, Joe YI, Alpert BK, Damrauer N, Doriese WB, Fatur S, Fowler JW, Hitlon G, Jimenez R, et al., Phys. Rev. X 2016, 6, 031047. 10.1103/PhysRevX.6.031047.

[48]. Ullom JN, Bennett DA, Supercond. Sci. Technol. 2015, 28(8), 084003. 10.1088/0953-2048/28/8/084003.

[49]. Doriese WB, Abbamonte P, Alpert BK, Bennett DA, Denison EV, Fang Y, Fischer DA, Fitzgerald CP, Fowler JW, Gard JD, Hays-Wehle JP, Hilton GC, Jaye C, McChesney JL, Miaja-Avila L, Morgan KM, Joe YI, O'Neil GC, Reintsema CD, Rodolakis F, Schmidt DR, Tatsuno H, Uhlig J, Vale LR, Ullom JN, Swetz DS, Rev. Sci. Instrum. 2017, 88(5), 053108. 10.1063/1.4983316.

[50]. Fowler JW, Alpert BK, Doriese WB, Joe YI, O'Neil GC, Ullom JN, Swetz DS, Low Temp J. Phys. 2016, 184, 374–381. 10.1007/s10909-015-1380-0.

[51]. Fowler JW, Alpert BK, Bennett DA, Doriese WB, Gard JD, Hilton GC, Hudson LT, Joe YI, Morgan KM, O'Neil GC, Reintsema CD, Schmidt DR, Swetz DS, Szabo CI, Ullom JN, Metrologia 2017, 54(4), 494–511. 10.1088/1681-7575/aa722f.

[52]. Chantler CT, Kinnane MN, Su CH, Kimpton JA, Phys. Rev. A At. Mol. Opt. Phys 2006, 73(1), 012508. 10.1103/PhysRevA.73.012508.

[53]. Chantler CT, Smale LF, Kimpton JA, Crosby DN, Kinnane MN, Illig AJ, Phys J. B At. Mol. Opt. Phys. 2013, 46(14), 145601. 10.1088/0953-4075/46/14/145601.

[54]. Hölzer G, Fritsch M, Deutsch M, Härtwig J, Förster E, Phys. Rev. A 1997, 56(6), 4554–4568. 10.1103/PhysRevA.56.4554.

[55]. Yan D, Divan R, Gades LM, Kenesei P, Madden TJ, Miceli A, Park J, Patel UM, Quaranta O, Sharma H, et al., Appl. Phys. Lett. 2017, 111, 192602. 10.1063/1.5001198.

[56]. Raju SS, Seetharami Reddy B, Murti MV, Mombasawala LA, X-Ray Spectrom 2007, 36(1), 35–41. 10.1002/xrs.

[57]. Mitra D, Sarkar M, Bhattacharya D, Natarajan LS, X-Ray Spectrom 2008, 37, 585–594. 10.1002/xrs.

[58]. Vinson J, Rehr JJ, Kas JJ, Shirley EL, Phys. Rev. B Condens. Matter Mater. Phys. 2011, 83(11), 115106. 10.1103/PhysRevB.83.115106.

[59]. Vinson J, Jach T, Elam WT, Denlinger JD, Phys. Rev. B Condens. Matter Mater. Phys 2014, 90(20), 205207. 10.1103/PhysRevB.90.205207.

[60]. Giannozzi P, Baroni S, Bonini N, Calandra M, Car R, Cavazzoni C, Ceresoli D, Chiarotti GL, Cococcioni M, Dabo I, Dal Corso A, de Gironcoli S, Fabris S, Fratesi G, Gebauer R, Gerstmann U, Gougoussis C, Kokalj A, Lazzeri M, Martin-Samos L, Marzari N, Mauri F, Mazzarello R, Paolini S, Pasquarello A, Paulatto L, Sbraccia C, Scandolo S, Sclauzero G, Seitsonen AP, Smogunov A, Umari P, Wentzcovitch RM, J. Phys. Condens. Matter 2009, 21(39), 395502. 10.1088/0953-8984/21/39/395502.

[61]. Ti Metal: AMCSD 0011195; TiO2 Anatase: AMCSD 0019093; TiO2 Rutile: AMCSD 0005164; TiO: COD 1101049; TiN: AMCSD 0011426; TiC: COD 5910091.

[62]. Gražulis S, Daškevič A, Merkys A, Chateigner D, Lutterotti L, Quirós M, Serebryanaya NR, Moeck P, Downs RT, Le Bail A, Nucleic Acids Res. 2012, 40(D1), 420–427. 10.1093/nar/gkr900.

[63]. Downs RT, Hall-Wallace M, Am. Mineral. 2003, 88(1), 247–250.

[64]. Krause MO, Oliver JH, J. Phys. Chem. Ref. Data 1979, 8(2), 329–338. 10.1063/1.555595.

[65]. Hébert C, Micron 2007, 38(1), 12–28. 10.1016/j.micron.2006.03.010. [PubMed: 16914318]

[66]. Weijs PJW, Czyzyk MT, Van Acker JF, Speier W, Goedkoop JB, Van Leuken H, Hendrix HJM, De Groot RA, Van Der Laan G, Buschow KHJ, et al., Phys. Rev. B 1990, 41(17), 11899–11910. 10.1103/PhysRevB.41.11899.

[67]. Diamant R, Huotari S, Hämäläinen K, Sharon R, Kao CC, Deutsch M, Phys. Rev. Lett. 2003, 91(19), 193001. 10.1103/PhysRevLett.91.193001.

[68]. Kawai J, Konishi T, Shimohara A, Gohshi Y, Spectrochim. Acta Part B At. Spectrosc. 1994, 49(7), 725–738. 10.1016/0584-8547(94)80064-2.

[69]. Mattern BA, Seidler GT, Haave M, Pacold JI, Gordon RA, Planillo J, Quintana J, Rusthoven B, Rev. Sci. Instrum. 2012, 83(2), 023901. 10.1063/1.3680598.

[70]. Reich C, Laperle CM, Li X, Ahr B, Benesch F, Rose-Petruck CG, Opt. Lett. 2007, 32(4), 427–429. [PubMed: 17356675]

[71]. Zamponi F, Ansari Z, Korff Schmising C, Rothhardt P, Zhavoronkov N, Woerner M, Elsaesser T, Bargheer M, Trobitzsch-Ryll T, Haschke M, Appl. Phys. A 2009, 96(1), 51–58. 10.1007/s00339-009-5171-9.

[72]. Weisshaupt J, Juvé V, Holtz M, Ku S, Woerner M, Elsaesser T, Ališauskas S, Pugžlys A, Baltuška A, Nat. Photonics 2014, 8(12), 927–930. 10.1038/nphoton.2014.256.

[73]. Schoonjans T, Brunetti A, Golosio B, Sanchez Del Rio M, Solé VA, Ferrero C, Vincze L, Spectrochim. Acta Part B At. Spectrosc. 2011, 66(11–12), 776–784. 10.1016/j.sab.2011.09.011.

[74]. Montel M, The X-ray microscopy with Catamegonic roof-shaped objective. in X-Ray Microscopy and Microradiography (Eds: Cosslett VE, Engstrom A, Pattee HH), Academic Press, New York, NY 1957.

[75]. Durkin M, Adams JS, Bandler SR, Chervenak JA, Chaudhuri S, Dawson CS, Denison EV, Doriese WB, Duff SM, Finkbeiner FM, FitzGerald CT, Fowler JW, Gard JD, Hilton GC, Irwin KD, Joe YI, Kelley RL, Kilbourne CA, Miniussi AR, Morgan KM, O'Neil GC, Pappas CG, Porter FS, Reintsema CD, Rudman DA, Sakai K, Smith SJ, Stevens RW, Swetz DS, Szypryt P, Ullom JN, Vale LR, Wakeham NA, Weber JC, Young BA, IEEE Trans. Appl. Supercond. 2019, 29(5), 2101005. 10.1109/TASC.2019.2904472.

[76]. Uhlig J, Doriese WB, Fowler JW, Swetz DS, Jaye C, Fischer DA, Reintsema CD, Bennett DA, Vale LR, Mandal U, et al., J. Synchrotron Radiat. 2015, 22(3), 766–775. 10.1107/S1600577515004312. [PubMed: 25931095]

[77]. Li D, Alpert BK, Becker DT, Bennett DA, Carini GA, Cho HM, Doriese WB, Dusatko JE, Fowler JW, Frisch JC, Gard JD, Guillet S, Hilton GC, Holmes MR, Irwin KD, Kotsubo V, Lee SJ, Mates JAB, Morgan KM, Nakahara K, Pappas CG, Reintsema CD, Schmidt DR, Smith SR, Swetz DS, Thayer JB, Titus CJ, Ullom JN, Vale LR, van Winkle DD, Wessels A, Zhang L, Low Temp J. Phys. 2018, 193(5–6), 1287–1297. 10.1007/s10909-018-2053-6.

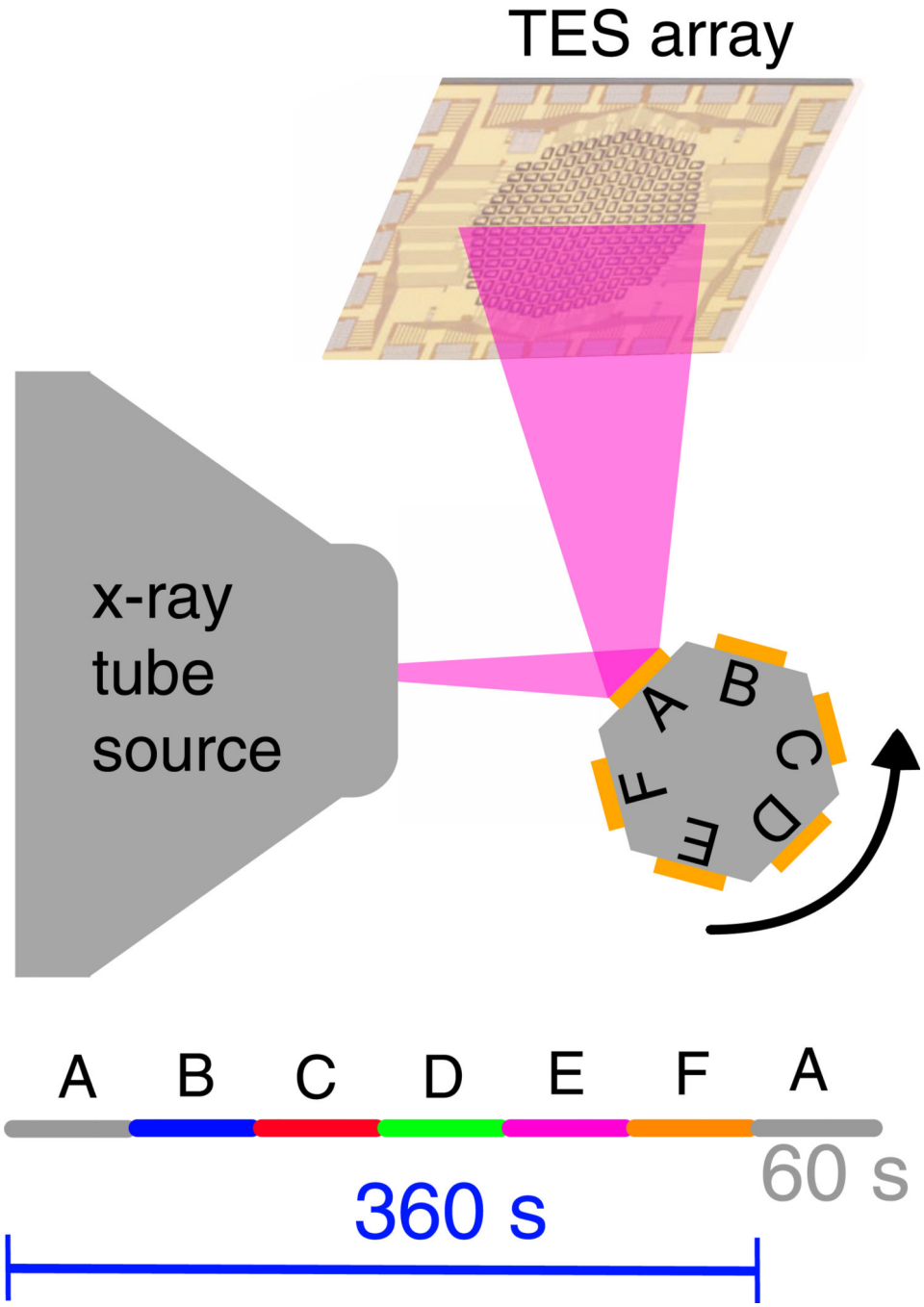

FIGURE 1.

Schematic of the sample switching XES setup. An X-ray tube source illuminates a six-sided sample holder one side at a time and the fluoresced X-rays are collected by a microcalorimeter array detector. Sides A through E contain a different titanium compound, while side F holds the calibration targets. This setup allows the measurement of calibration lines in every complete rotation

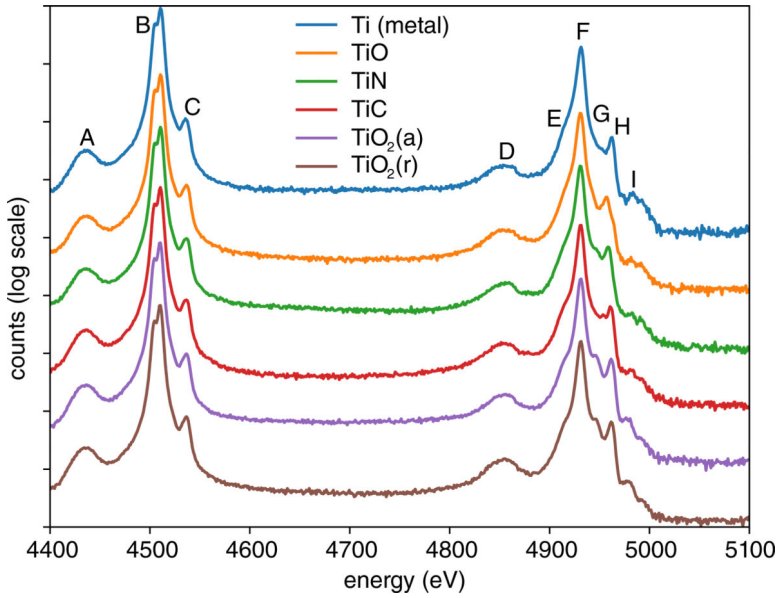

FIGURE 2.

XES spectra for the different titanium compounds. The labeled features in the spectrum denote: A: detector artifact from Kα photons absorbed in the underlying SiN, B: $K\alpha_{1,2}$ lines, C: Kα satellites, also called $K_\alpha L^1$, D: detector artifact from Kβ photons absorbed in the underlying SiN, E: Kβ' line, F: $K\beta_{1,3}$ lines, G: Kβ" lines, H: $K\beta_{2,5}$ lines, and I: $K_\beta L^1$ lines. The energy resolution in the Kα region is 3.8 ± 0.1 and 4.0 ± 0.1 eV in the Kβ region

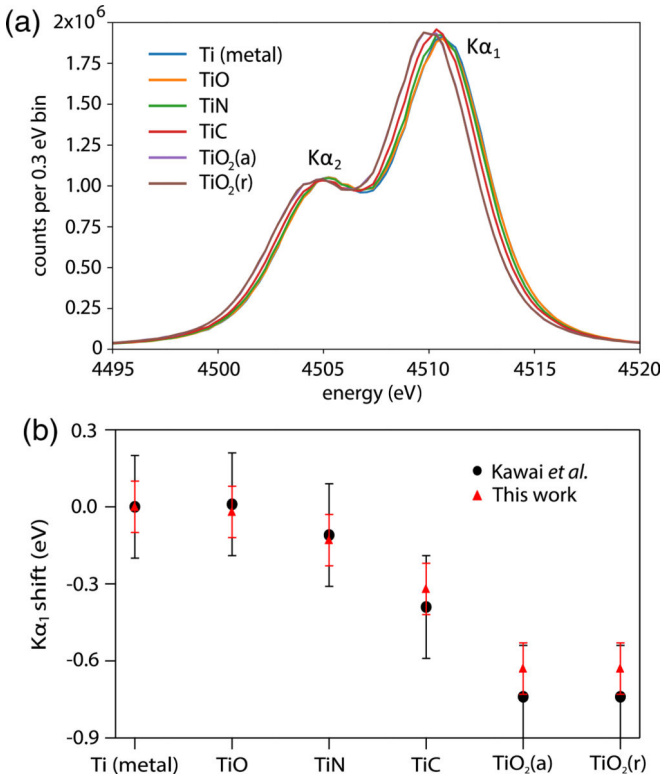

FIGURE 3.

(a) Measured Ti $K\alpha_{1,2}$ XES spectra of the different compounds. Even with an energy resolution of 3.8 ± 0.1 eV, a shift of the Kα features is clearly observed in the spectra. (b) $K\alpha_1$ shift with respect to the Ti metal $K\alpha_1$ position. Our measurements are compared to previously published results (see Kawai et al.[68]) and are consistent with the idea that a shift of the $K\alpha_1$ peak to lower energies correlates with the decrease of 3d electrons. Errors bars for our data are primarily systematic (see Supporting Information, Data S1)

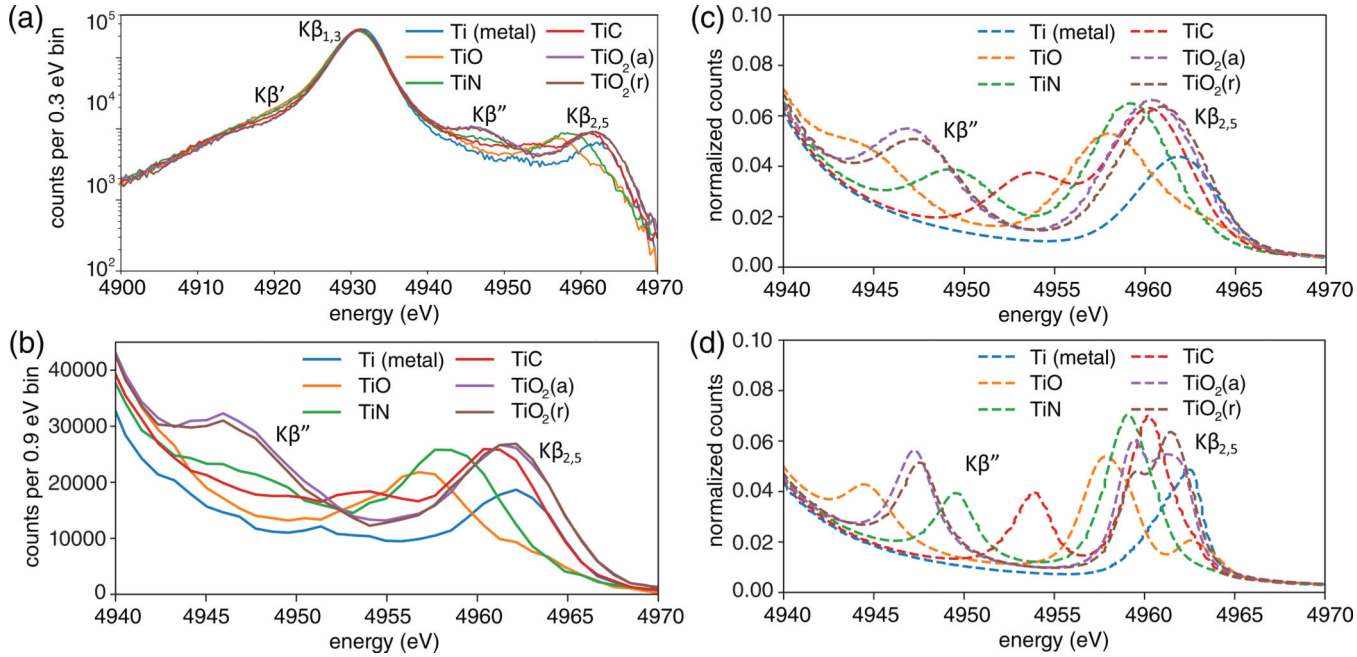

FIGURE 4.

(a) Titanium Kβ main and satellite XES spectra. The energy resolution in this region of the spectrum is 4.0 ± 0.1 eV. (b) Valence-to-core XES spectra using the microcalorimeter array detectors and (c) OCEAN simulated vtc-XES spectra including instrument and lifetime broadening. (d) OCEAN simulated vtc-XES spectra including lifetime broadening only. The shifts in the $K\beta_{2,5}$ features are clearly observable in the microcalorimeter data as well as the presence of the Kβ" peaks. See Table 1 for energy shift values and a comparison between various measurements and the OCEAN simulations

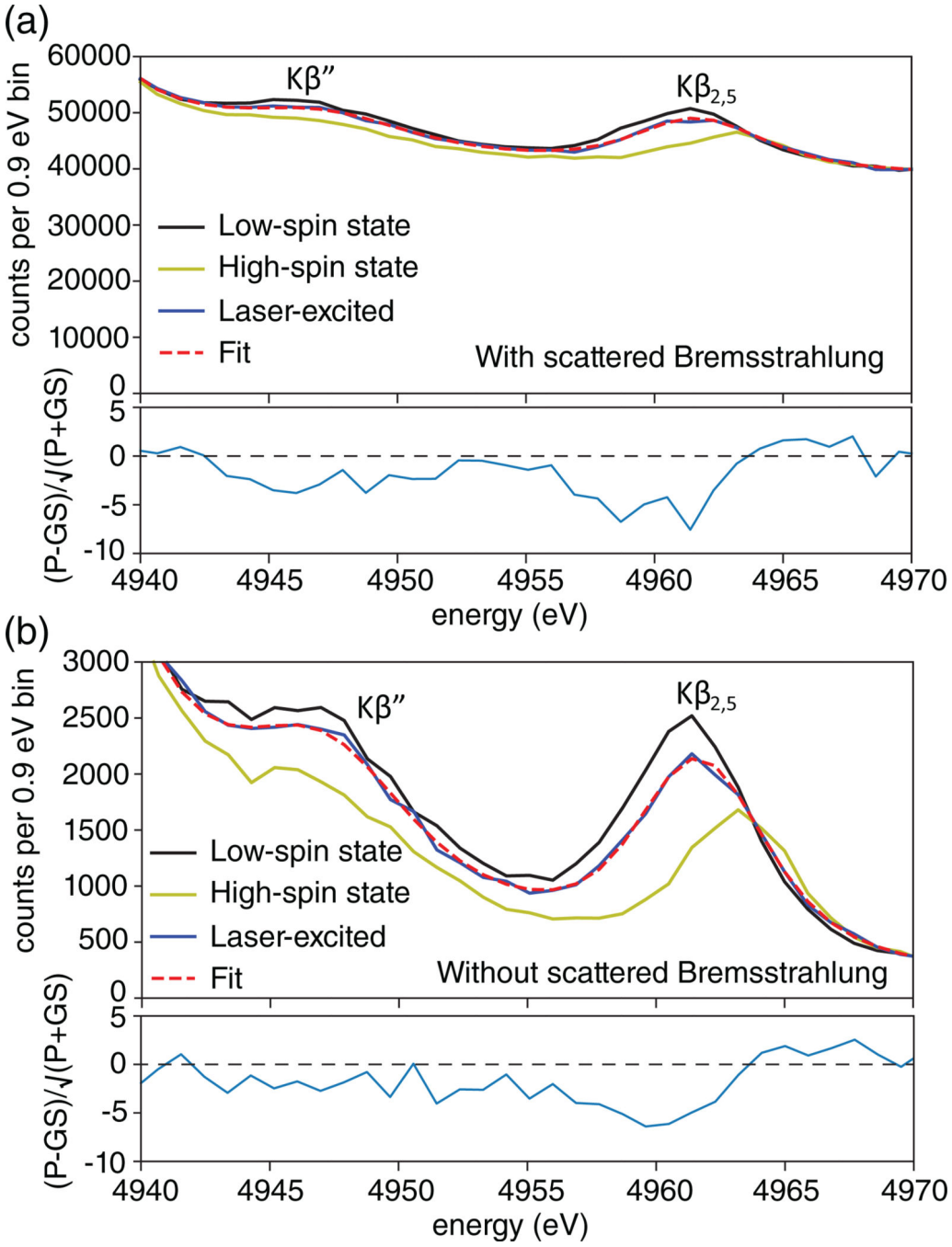

FIGURE 5.

Calculated vtc-XES spectra and signal-to-noise assuming the use of a water-jet laser plasma source and (a) a polycapillary X-ray optic with 1×10^7 counts in the vtc region, and (b) a monochromatic focusing optic with 5×10^5 counts in the vtc region, spanning from 4,940 to 4,970 eV. The main difference between the plots is the fact that the scattered Bremsstrahlung signal is high in (a) and close to zero in (b), see text for a discussion of acquisition times.

The axis label (P-GS)/√(P + GS) represents the difference between the laser-excited (pump) spectra and the ground-state (low-spin) spectra in units of *standard deviation*

TABLE 1.

Energy separation between the $K\beta_{1,3}$ and $K\beta_{2,5}$ peaks for the different Ti compounds

Sample (oxidation state)	$K\beta_{2,5} - K\beta_{1,3}$ (eV)	Reference
Ti	30.3 ± 0.1	Microcalorimeter
	31.0	OCEAN
	30.7 ± 0.3	Wansleben[23]
TiO (II)	26.1 ± 0.1	Microcalorimeter
	26.2	OCEAN
	26.2 ± 0.1	Synchrotron
	26.3 ± 0.5	Mandić[21]
	25.3 ± 0.3	Wansleben
TiN (III)	27.4 ± 0.1	Microcalorimeter
	28.2	OCEAN
	27.8 ± 0.1	Synchrotron
	31.6 ± 0.5	Mandić
TiC (IV)	29.8 ± 0.1	Microcalorimeter
	29.1	OCEAN
	30.3 ± 0.1	Synchrotron
	29.3 ± 0.5	Mandić
TiO_2 anatase (IV)	30.1 ± 0.1	Microcalorimeter
	29.3	OCEAN
	29.2 ± 0.1	Synchrotron
	29.8 ± 0.5[a]	Mandić
	29.9 ± 0.2[a]	Wansleben
TiO_2 rutile (IV)	30.1 ± 0.1	Microcalorimeter
	29.7	OCEAN
	29.2 ± 0.1	Synchrotron

Note: Our microcalorimeter array results are consistent with measurements performed at the synchrotron, OCEAN simulations, and previously published results. The discrepancy with the literature result on the energy separation for the TiN sample is discussed in the main text, while the Supplementary Information (Data S1) contains a discussion on the uncertainty values.

[a]Mandić et al.[21] and Wansleben et al.[23] published energy separations for TiO_2, but it is not mentioned whether the crystal structure is anatase or rutile.